

Article

Halogen-Bonding-Driven Self-Assembly of Solvates of Tetrabromoterephthalic Acid

Nucharee Chongboriboon¹, Kodchakorn Samakun¹, Winya Dungkaew², Filip Kielar³,
Mongkol Sukwattanasinitt⁴ and Kittipong Chainok^{1,*} 

¹ Thammasat University Research Unit in Multifunctional Crystalline Materials and Applications (TU-MCMA), Faculty of Science and Technology, Thammasat University, Pathum Thani 12121, Thailand; nucharee.chon@dome.tu.ac.th (N.C.); kodchakorn.sama@dome.tu.ac.th (K.S.)

² Department of Chemistry, Faculty of Science, Mahasarakham University, Mahasarakham 44150, Thailand; winya.d@msu.ac.th

³ Department of Chemistry, Faculty of Science, Naresuan University, Phitsanulok 65000, Thailand; filipk@nu.ac.th

⁴ Department of Chemistry, Faculty of Science, Chulalongkorn University, Bangkok 10330, Thailand; mongkol.s@chula.ac.th

* Correspondence: kc@tu.ac.th; Tel.: +66-86-339-5079

Abstract: Halogen bonding is one of the most interesting noncovalent attractions capable of self-assembly and recognition processes in both solution and solid phase. In this contribution, we report on the formation of two solvates of tetrabromoterephthalic acid (H_2Br_4tp) with acetonitrile ($MeCN$) and methanol ($MeOH$) viz. $H_2Br_4tp \cdot 2MeCN$ (1_{MeCN}) and $H_2Br_4tp \cdot 2MeOH$ (2_{MeOH}). The host structures of both 1_{MeCN} and 2_{MeOH} are assembled via the occurrence of simultaneous $Br \cdots Br$, $Br \cdots O$, and $Br \cdots \pi$ halogen bonding interactions, existing between the H_2Br_4tp molecular tectons. Among them, the cooperative effect of the dominant halogen bond in combination with hydrogen bonding interactions gave rise to different supramolecular assemblies, whereas the strength of the halogen bond depends on the type of hydrogen bond between the molecules of H_2Br_4tp and the solvents. These materials show a reversible release/resorption of solvent molecules accompanied by evident crystallographic phase transitions.

Keywords: halogen bonds; hydrogen bonds; solvate; structural phase transition; Hirschfeld surface; tetrabromoterephthalic acid



Citation: Chongboriboon, N.; Samakun, K.; Dungkaew, W.; Kielar, F.; Sukwattanasinitt, M.; Chainok, K. Halogen-Bonding-Driven Self-Assembly of Solvates of Tetrabromoterephthalic Acid. *Crystals* **2021**, *11*, 198. <https://doi.org/10.3390/cryst11020198>

Academic Editors: Maija Nissinen and Atash V. Gurbanov

Received: 12 January 2021

Accepted: 11 February 2021

Published: 18 February 2021

Publisher's Note: MDPI stays neutral with regard to jurisdictional claims in published maps and institutional affiliations.



Copyright: © 2021 by the authors. Licensee MDPI, Basel, Switzerland. This article is an open access article distributed under the terms and conditions of the Creative Commons Attribution (CC BY) license (<https://creativecommons.org/licenses/by/4.0/>).

1. Introduction

Supramolecular interactions have been extensively investigated due to their importance in governing various interesting physical properties as well as chemical and biological assemblies [1–3]. Halogen bonding (XB) is emerging as one of the prominent intermolecular interactions that takes place between the sigma (σ)-hole of the polarizable halogen atom (Lewis acid, XB donor) and the electron-rich atom or π -electron system (Lewis base, XB acceptor) [4,5]. Generally, the XB interaction is presented as $D-Y \cdots A$, where $D-Y$ and A are the XB donor and XB acceptor, respectively. This type of interaction is highly directional and exhibits highly predictable bond geometries in the solid state. Theoretical calculations have suggested that the strength of the halogen bonding interaction energies is comparable to that of the ubiquitous hydrogen bond [6] and that the strength of the XB donor increases in the following order as the XB donor ability increases: $F < Cl < Br < I$ [7]. These features suggest that the halogen bonding interactions could be used as a crystal engineering tool for designing and developing novel functional materials in the crystalline state [8].

Recently, halogen bond-based supramolecular synthons have been used to construct an exciting class of porous organic materials named halogen-bonded organic frameworks (XBOFs), which are self-assembled from pure organic building blocks (tectons) [9–11]. Compared with analogous materials such as covalent organic frameworks (COFs) and

metal-organic frameworks (MOFs), where the frameworks are built using strong covalent bonds [12], the extended supramolecular frameworks of XBOFs are even more flexible, allowing the inclusion of guests with specific intermolecular interactions. In this regard, the combination of suitable molecular tectons and specific halogen bond synthons is important for the creation of new functional XBOF materials with specific applications. Among the various organic tectons, iodobenzene derivatives and pyridine moieties are the most widely studied in directing the formation of XBOF structures through strong and directional I \cdots N synthons [13–15]. For instance, the group of B. Ji and D. Deng recently used the molecular tectons of 1,4-difluoro-2,3,5,6-tetraiodobenzene and 1,2,4,5-tetra(4-pyridyl)benzene to construct a series of XBOFs [16]. The crystal structure determination revealed that the strong and directional I \cdots N interactions (3.002 and 3.096 Å) between the respective components is mainly responsible for the formation of flexible frameworks, possessing large flexible breathing 1D channels. Notably, the flexible frameworks of these materials show selective recognition for aromatic guest molecules.

In this work, the tetrabromoterephthalic acid (H₂Br₄tp) was employed as a molecular building block to synthesize new solvate crystals. This molecule contains two carboxyl and four bromo groups with versatile tectons in self-complementary XB modules bearing both XB donor and XB acceptor sites. Crystallization of H₂Br₄tp from acetonitrile (MeCN) and methanol (MeOH) yielded two solvates with a 1:2 molar ratio viz. H₂Br₄tp·2MeCN (**1**_{MeCN}) and H₂Br₄tp·2MeOH (**2**_{MeOH}). As expected, the functional groups of the H₂Br₄tp tectons can be involved in self-complementary Br \cdots Br, Br \cdots O, and Br \cdots π halogen bonding interactions, resulting in the formation of 2D XBOFs. Moreover, the 2D assemblies can form the inclusion of solvents MeCN and MeOH assembled through both strong and weak hydrogen bonding interactions. These materials can undergo many cycles of release/resorption of solvent molecules, exhibiting crystallographic phase changes between the solvated (*P*-1 for **1**_{MeCN} and *P*2₁/*c* for **2**_{MeOH}) and unsolvated (*C*2/*m* for H₂Br₄tp [17]) crystals.

2. Experimental Setup

2.1. Materials and Methods

All chemicals and solvents, i.e., H₂Br₄tp, MeCN, and MeOH, were reagent grade and were used without further purification. Elemental (C, H, and N) analysis was determined with a LECO CHNS 932 elemental analyzer. Powder X-ray diffraction (PXRD) measurements were carried out on a Bruker D8 ADVANCE X-ray powder diffractometer using Cu K α (λ = 1.5418 Å). FT-IR spectra were recorded on a Perkin-Elmer model Spectrum GX FT-IR spectrometer using attenuated total reflection (ATR) mode in the range of 650–4000 cm⁻¹. Thermogravimetric analyses (TGA) were carried out using a Mettler Toledo TGA/DSC3+ from 30–500 °C with a heating rate of 10 °C min⁻¹, under nitrogen atmosphere.

2.2. Synthesis and Crystallization of H₂Br₄tp·2MeCN (**1**_{MeCN})

A mixture of H₂Br₄tp (5 mg) and MeCN (2 ml) was added into a 25 mL Teflon-lined reactor, sealed in a stainless-steel autoclave, and placed in an oven. The mixture was heated from room temperature to 110 °C under autogenous pressure for 1 h and then cooled down to room temperature. Colorless block-shaped crystals of **1**_{MeCN} were obtained. Anal. calc. for C₁₂H₈Br₄N₂O₄: C, 25.56; H, 1.43; N, 4.97%. Found: C, 25.60; H, 1.43; N, 4.82%. FT-IR (ATR, ν /cm⁻¹, s for strong, m medium, w weak): 3514w, 3421w, 3149w, 1571s, 1415s, 1324s, 1570s, 1182w, 1069m, 919w.

2.3. Synthesis and Crystallization of H₂Br₄tp·2MeOH (**2**_{MeOH})

Colorless block-shaped crystals of **2**_{MeOH} were synthesized by a similar procedure as **1**_{MeCN} above except that MeCN was replaced with MeOH. Anal. calc. for C₁₀H₁₀Br₄O₆: C, 22.01; H, 1.85%. Found: C, 22.26; H, 1.91%. FT-IR (ATR, ν /cm⁻¹): 3514w, 3421w, 3149w, 1571s, 1415s, 1324s, 1570s, 1182w, 1069m, 919w.

2.4. X-ray Crystallography

Suitable crystals of **1_{MeCN}** and **2_{MeOH}** were carefully selected and mounted on MiTeGen micromounts using paratone-*N* oil. X-ray diffraction data were collected using a Bruker D8 QUEST CMOS PHOTON II with graphite monochromated Mo- $K\alpha$ ($\lambda = 0.71073 \text{ \AA}$) radiation at 296(2) K. Data reduction was performed using SAINT, and the SADABS scaling algorithm [18] was used for absorption correction. The structure was solved with the ShelXT structure solution program using combined Patterson and dual-space recycling methods [19]. The structure was refined by least squares using ShelXL [20]. All non-H atoms were refined anisotropically. The H atoms of solvent molecules were positioned geometrically with C–H = 0.96 \AA and refined using a riding model (AFIX137 for methyl H atom in ShelXL program) with fixed displacement parameters $U_{\text{iso}}(\text{H}) = 1.5U_{\text{eq}}(\text{C})$. The O–H hydrogen atoms were located on difference Fourier maps but refined with O–H = $0.82 \pm 0.01 \text{ \AA}$ with $U_{\text{iso}}(\text{H}) = 1.5U_{\text{eq}}(\text{O})$. A summary of crystal data and structural refinement parameters for **1_{MeCN}** and **2_{MeOH}** is given in Table 1.

Table 1. Crystal data and structure refinement for **1_{MeCN}** and **2_{MeOH}**.

Compound	H ₂ Br ₄ tp·2MeCN (1_{MeCN})	H ₂ Br ₄ tp·2MeOH (2_{MeOH})
Empirical formula	C ₁₂ H ₈ Br ₄ N ₂ O ₄	C ₁₀ H ₁₀ Br ₄ O ₆
Formula weight	563.84	545.82
Temperature (K)	296(2)	296(2)
Crystal system	Triclinic	Monoclinic
Space group	<i>P</i> -1	<i>P</i> 2 ₁ / <i>c</i>
<i>a</i> (\AA)	6.1577(6)	11.8461(11)
<i>b</i> (\AA)	8.3463(8)	9.2213(8)
<i>c</i> (\AA)	9.2327(9)	15.1000(14)
α ($^\circ$)	68.241(3)	90
β ($^\circ$)	78.863(4)	107.840(3)
γ ($^\circ$)	84.436(4)	90
<i>V</i> (\AA^3)	432.23(7)	1570.2(2)
<i>Z</i>	1	4
ρ_{calc} (g/cm ³)	2.166	2.309
μ (mm ⁻¹)	9.327	10.271
<i>F</i> (000)	266	1032
λ (\AA)	0.71073 (Mo- $K\alpha$)	0.71073 (Mo- $K\alpha$)
θ range ($^\circ$)	3.4–32.1	2.8–32.1
Reflections collected	17952	50246
Independent reflections	3149	5490
<i>R</i> _{int} , <i>R</i> _{sigma}	0.0566, 0.0429	0.0968, 0.0650
Data/restraints/parameters	3149/1/106	5490/4/200
Goodness-of-fit on <i>F</i> ²	1.028	1.025
<i>R</i> ₁ , <i>wR</i> ₂ [<i>I</i> > 2 σ (<i>I</i>)]	0.0427, 0.0731	0.0519, 0.0944
<i>R</i> ₁ , <i>wR</i> ₂ [all data]	0.0909, 0.0871	0.1189, 0.1167
$\Delta\rho_{\text{max}}$, $\Delta\rho_{\text{min}}$ (e \AA^{-3})	0.57, −0.69	0.93, −1.14
CCDC number	2005667	2005668

3. Results and Discussion

3.1. Structural Description

Colorless block-shaped crystals of **1_{MeCN}** and **2_{MeOH}** were obtained upon the crystallization of H₂Br₄tp from the solvents MeCN and MeOH at 110 °C for 1 h in a 25 mL Teflon-lined stainless-steel container. Alternatively, single crystals of these two solvates can also easily be grown by dissolving H₂Br₄tp in each respective solvent and by allowing them to crystallize by slow evaporation at room temperature for 24 h. The single-crystal X-ray diffraction analysis revealed that the solvates crystallize in the centrosymmetric system with space groups *P*-1 and *P*2₁/*c* for **1_{MeCN}** and **2_{MeOH}**, respectively. These solvates have a similar 1:2 stoichiometric ratio of H₂Br₄tp and solvent molecules. Figure 1 shows the molecular structure with the atomic numbering schemes of the solvates. The asymmetric

unit of 1_{MeCN} contains half a molecule of $\text{H}_2\text{Br}_4\text{tp}$ located at a center of inversion and one MeCN molecule. In contrast, there are one $\text{H}_2\text{Br}_4\text{tp}$ molecule and two MeOH molecules in the asymmetric unit of 2_{MeOH} .

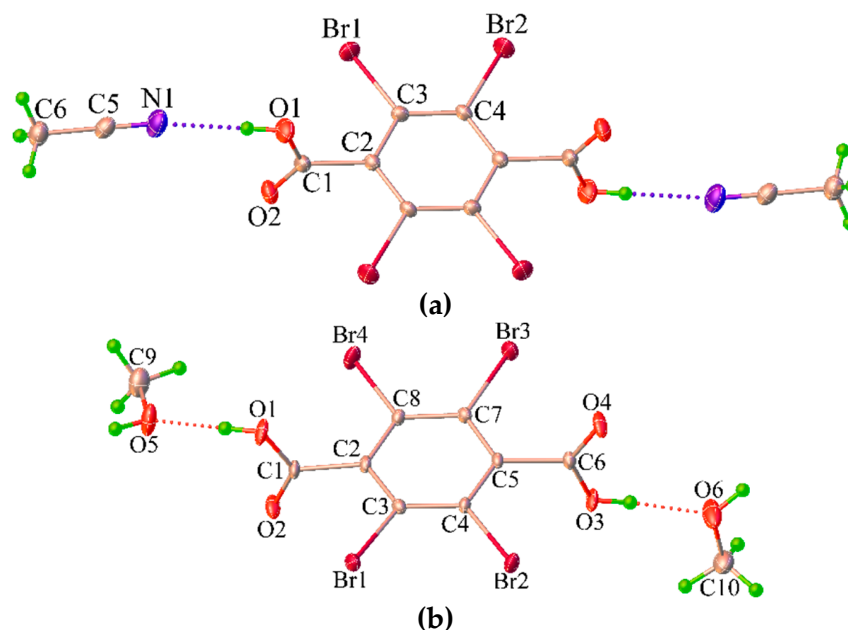


Figure 1. The molecular structures with 30% probability displacement ellipsoids and atom numbering schemes of (a) 1_{MeCN} and (b) 2_{MeOH} .

In the crystal of 1_{MeCN} , the $\text{H}_2\text{Br}_4\text{tp}$ molecules are linked by $\text{Br}\cdots\text{O}$ halogen bond and weak van der Waals (vdW) $\text{O}\cdots\text{O}$ interactions to generate a two-dimensional (2D) sheet structure along the a axis (Figure 2a). The observed $\text{Br}\cdots\text{O}$ halogen bonding interaction (3.270(3) Å) between bromine atom and the oxygen carbonyl atom in 1_{MeCN} is $\approx 3\%$ shorter than the sum of the vdW radii of the Br and O atoms (3.37 Å) [21], and the $\text{C}-\text{Br}\cdots\text{O}$ bond angle (155.3°) is slightly bent. In contrast, the non-bonded $\text{O}\cdots\text{O}$ distance (3.038(6) Å) between the oxygen atoms of the carboxyl groups is almost the same as the sum of the vdW radii of the two oxygen atoms (3.04 Å). Apparently, the solvent MeCN molecules are located between the 2D layered sheets and participate in $\text{O}-\text{H}\cdots\text{N}$ and $\text{C}-\text{H}\cdots\text{O}$ hydrogen bonding interactions (Table S1) in the tetrameric motif with graph set notation $R^4_4(16)$ [22] (Figure 2b). Such interactions along with additional weak type I $\text{Br}\cdots\text{Br}$ halogen bonds and $\text{Br}\cdots\pi$ contacts ($\text{Br}\cdots\text{C} \approx 3.5$ Å) [23] link the 2D sheets into a 3D supramolecular architecture. Further investigation of the packing structure found that the centroid–centroid distances between the stacked $\text{C}\equiv\text{N}$ group of the MeCN molecule and the aromatic ring of the $\text{H}_2\text{Br}_4\text{tp}$ molecule is 3.997(5) Å, which indicates a weak $\pi-\pi$ interaction [24]. This also contributes to the packing stabilization of the solvate 1_{MeCN} . The geometric parameters for the halogen bonds and the hydrogen bonds of the solvates are provided in Table 2 and Table S1 (Supplementary Materials), respectively.

For 2_{MeOH} , the $\text{H}_2\text{Br}_4\text{tp}$ molecules are assembled together by $\text{Br}\cdots\text{O}$ halogen bonding (3.043(3) and 3.087(3) Å) and $\text{O}\cdots\text{O}$ (3.022(3) Å) interactions similar to that of 1_{MeCN} above, giving rise to a 2D sheet structure approximately along the a axis, as illustrated in Figure 3a. However, unlike 1_{MeCN} , several $\text{Br}\cdots\text{Br}$ interactions (3.7233(7)–3.8871(8) Å) of types I and II exist in the crystal structure of 2_{MeOH} (Figure 3b), and these values are slightly longer than the sum of the vdW radii, indicative of weak interactions. It should also be noted that the $\text{Br}\cdots\text{O}$ distances in 2_{MeOH} (Table 2) are much shorter than those observed for 1_{MeCN} . This is possibly due to the influence of the geometry of the MeOH molecules on packing. $\text{H}_2\text{Br}_4\text{tp}$ and the MeOH molecules can behave as either hydrogen bond donor or acceptor sites similar to that of 1_{MeCN} and interact with each other via the $\text{O}-\text{H}\cdots\text{O}$ and $\text{C}-\text{H}\cdots\text{O}$ hydrogen bonding interactions (Table S1), leading to the formation of the

tetrameric hydrogen bonding motif with an $R_4^4(12)$ graph set (Figure 3c). These interactions serve to connect the sheets into a 3D architecture.

Table 2. Parameters of the C–Br \cdots X halogen bonds for **1**_{MeCN} and **2**_{MeOH}.

C–Br \cdots X	d(Br \cdots X) (Å)	\angle (C–Br \cdots X) (°)	Symmetry Code
1 _{MeCN}			
C3–Br1 \cdots Br2	3.9434(7)	85.26(10)	$-x, -y, 1 - z$
C4–Br2 \cdots O2	3.270(3)	155.24(11)	$x, y, z - 1$
2 _{MeOH}			
C3–Br1 \cdots O4	3.087(4)	173.41(14)	$1 - x, 1/2 + y, 3/2 - z$
C4–Br2 \cdots O1	3.043(3)	177.69(15)	$1 - x, 1/2 + y, 3/2 - z$
C4–Br2 \cdots Br3	3.7233(7)	89.77(13)	$x, 1/2 - y, z + 1/2$
C4–Br2 \cdots Br4	3.8507(8)	119.49(13)	$x, 1/2 - y, z + 1/2$
C8–Br3 \cdots Br1	3.7989(7)	176.35(13)	$x, 1/2 - y, z - 1/2$
C8–Br3 \cdots Br3	3.7994(11)	77.52(13)	$1 - x, -y, 1 - z$
C8–Br3 \cdots Br4	3.8871(8)	103.15(13)	$1 - x, -y, 1 - z$

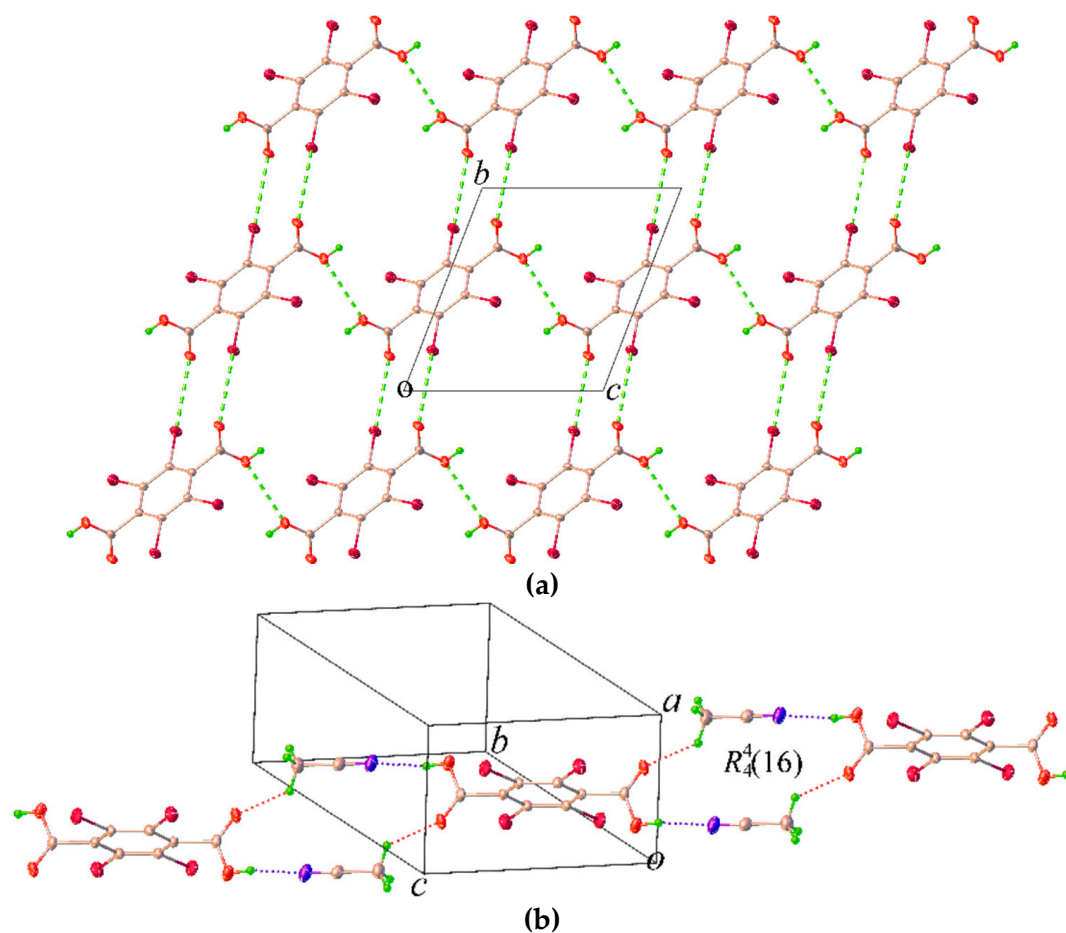


Figure 2. Partial views of (a) the 2D sheet constructed by halogen bond Br \cdots O and vdW O \cdots O interactions (dashed lines) between the H₂Br₄tp molecules and (b) the 1D chain formed by O–H \cdots N and C–H \cdots O interactions (dashed lines) with an $R_4^4(16)$ graph set existing between the H₂Br₄tp and the MeCN molecules in **1**_{MeCN}.

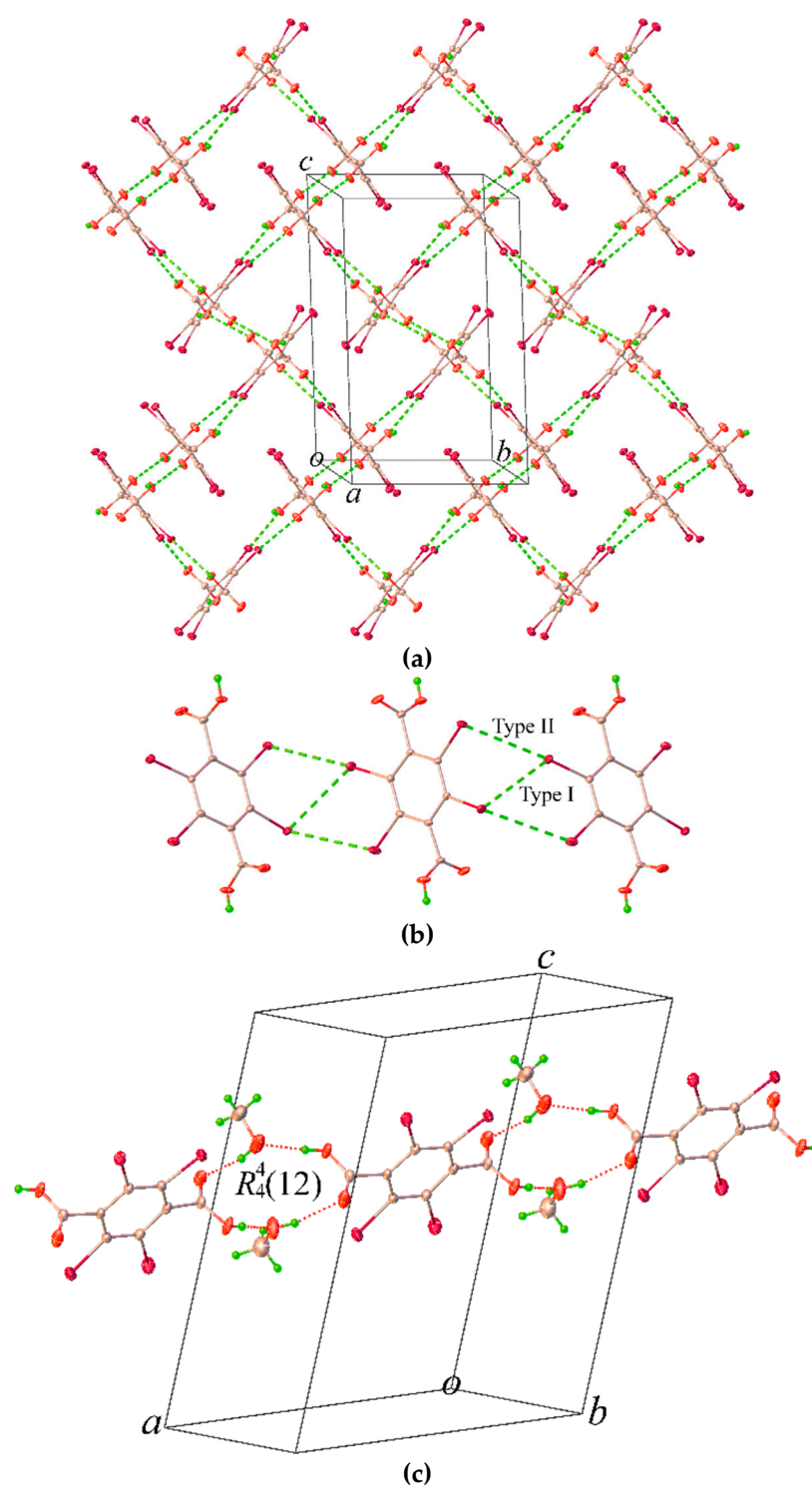


Figure 3. Partial views of (a) the 2D sheet constructed by Br \cdots O and O \cdots O interactions (dashed lines) between the H₂Br₄tp molecules, (b) the Br \cdots Br interactions of types I and II, and (c) the 1D chain formed by O–H \cdots O and C–H \cdots O interactions (dashed lines) with an $R_4^4(12)$ graph set existing between the H₂Br₄tp and the MeOH molecules in **2MeOH**.

Figure 4 depicts the packing diagrams and the contact surface of the channels viewed along the *a* and *b* axes for **1MeCN** and **2MeOH**, respectively. Although both solvates have the same composition and stoichiometry, it can clearly be seen that different solvents lead to differences in molecular orientation within the crystal packing. This can be attributed to the nature (size, shape, and intermolecular interaction capabilities) and the different

roles of solvent molecules during supramolecular framework assembly. It appears that the space accommodating the MeCN molecule in 1_{MeCN} has a cylinder-like geometry (1D channel along the a axis) with discontinuous voids (Figure 4a). For 2_{MeOH} , the space occupied by the MeOH molecules shows continuous in-void volume maps (Figure 4b) that propagate in two directions (the ac plane). Despite the different packing arrangements, either solvent MeCN or MeOH molecules are involved in the hydrogen bonding with similar tetrameric hydrogen-bonding motifs as described above. A comparison of the packing efficiency (Ck) using PLATON [25] revealed that 1_{MeCN} ($Ck = 46.9\%$) possesses a lower packing efficiency than that of 2_{MeOH} ($Ck = 52.1\%$). This result demonstrates that the components in the solvate 2_{MeOH} pack more tightly, which may be attributed to the presence of numerous $\text{Br}\cdots\text{O}$, $\text{Br}\cdots\text{Br}$, and $\text{Br}\cdots\pi$ halogen bonding and classical $\text{O}\cdots\text{H}\cdots\text{O}$ hydrogen bonding interactions. Furthermore, the potential solvent-accessible void space after the removal of solvent molecules, also calculated using PLATON, was estimated to be $\approx 34.8\%$ and 30.4% for 1_{MeCN} and 2_{MeOH} , respectively. In this regard, the 2D supramolecular frameworks with visualized surfaces of void structures of these solvates may potentially serve as a stable soft host framework for polar organic molecules.

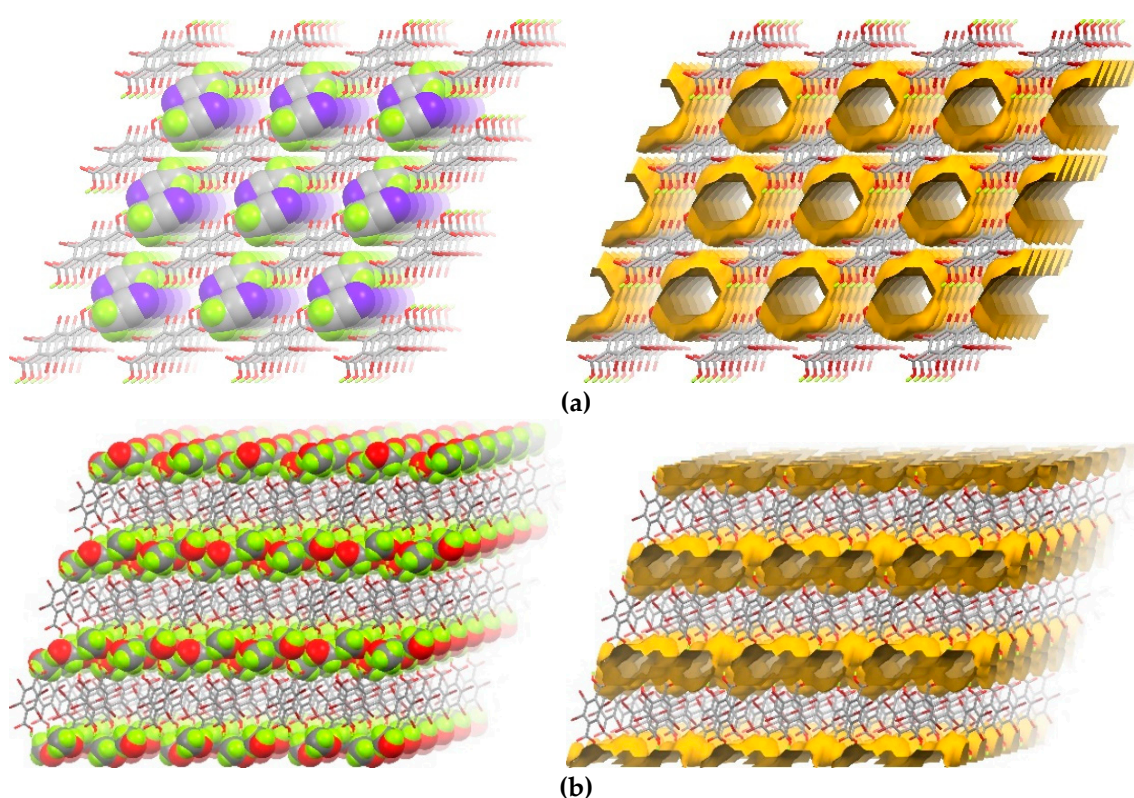


Figure 4. Partial views of crystal packing with solvent molecules displayed using the space-filling model and the contact surface of the cavities calculated in mercury using a probe radius of 1.2 for (a) 1_{MeCN} and (b) 2_{MeOH} .

Additionally, given the abundance of bromine atoms in the $\text{H}_2\text{Br}_4\text{tp}$ molecular tectons, perhaps it is not surprising that $\text{Br}\cdots\text{O}$, $\text{Br}\cdots\text{Br}$, and $\text{Br}\cdots\pi$ synthons were the most frequently found halogen bonding motifs in 1_{MeCN} and 2_{MeOH} . Our previous studies also indicated that this type of interaction was common in $\text{H}_2\text{Br}_4\text{tp}$ solvates with acetone, ethanol, dimethyl sulfoxide, and ethylene glycol solvents [23] and is mainly responsible for the formation of their layered sheets. Despite this, each solvate exhibits subtle differences in overall packing due to different hydrogen bonding and the orientation of the solvent molecules. Notably, $\text{H}_2\text{Br}_4\text{tp}$ can selectively accommodate MeOH molecules relative to other solvents. This is probably related to the molecular shape and size, the acidity scale, as well as some specific intermolecular interactions.

3.2. Hirshfeld Surface Analysis

The nature of the intermolecular interactions between the molecules within the crystal structure of the solvates **1**_{MeCN} and **2**_{MeOH} was further quantified and visualized by Hirshfeld surfaces [26] and their associated 2D fingerprint plots [27] performed with *CrystalExplorer* [28]. The shorter and longer contacts on the Hirshfeld surfaces are indicated as red and blue spots, respectively, while white spots indicate contacts with distances approximately equal to the sum of the vdW radii. The function d_{norm} (normalized distance) is a ratio enclosing the distances of any surface point to the nearest interior (d_i) and exterior (d_e) atom and the vdW radii of the atoms. As can be seen from the structural analysis above, the bromine atoms of the host $\text{H}_2\text{Br}_4\text{tp}$ molecules are involved in $\text{Br}\cdots\text{Br}$, $\text{Br}\cdots\text{O}$, and $\text{Br}\cdots\pi$ halogen bonding interactions. The contributions of such interatomic contacts to the d_{norm} surface in these solvates are compared and shown in Figure 5.

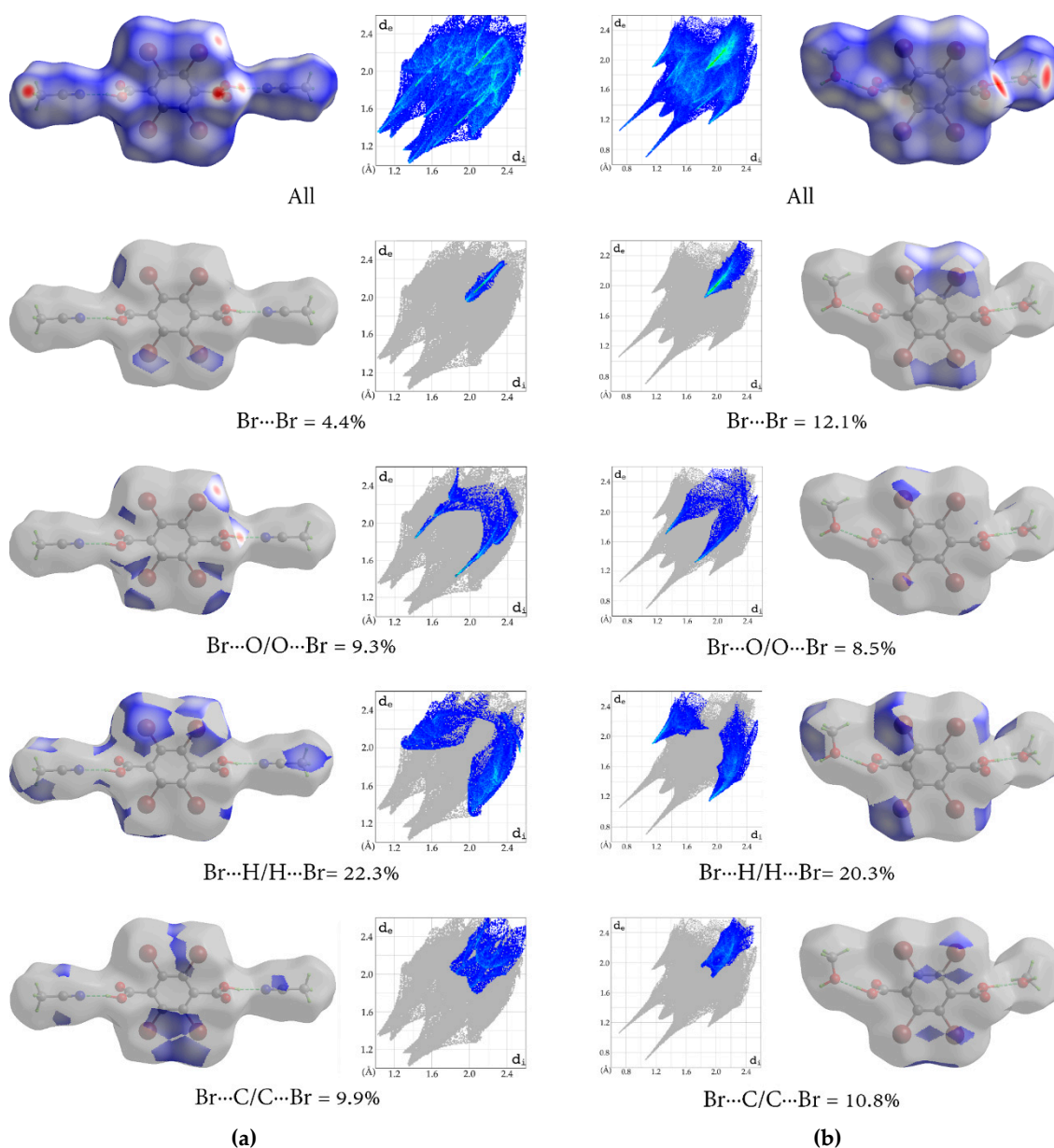


Figure 5. Two-dimensional fingerprint plots of (a) **1**_{MeCN} and (b) **2**_{MeOH}, showing all interactions, and those delineated into intermolecular contacts involving bromine atoms.

It is evident that the 2D fingerprint plots of all contacts among these solvates differ significantly due to the differences in packing arrangements and intermolecular interactions in the solid state. Specifically, there is major significant difference in the Br...Br contact, which comprises 4.4% and 12.1% of the d_{norm} surface for **1**_{MeCN} and **2**_{MeOH}, respectively, while the Br...O contacts show quite similar contributions to the surface (9.3% for **1**_{MeCN} and 8.5% for **2**_{MeOH}). Apparently, both solvates feature Br...C/C...Br contacts (9.9% for **1**_{MeCN} and 10.8% for **2**_{MeOH}), which are manifested as weak Br... π contacts. The Br...H/H...Br contacts also have a significant contribution towards the crystal stabilization of these solvates (22.3% for **1**_{MeCN} and 20.3% for **2**_{MeOH}). It should be noted that O...O contacts for these solvates contribute a negligible percentages (1.8% for **1**_{MeCN} and 1.1% for **2**_{MeOH}) towards the total surface area. Furthermore, the dominant interactions between H and O or N atoms, corresponding to the discussed hydrogen bonding interactions have also been visualized by selecting the host H₂Br₄tp molecules as the object. As can be clearly seen from Figure 6, these solvates exhibit red spots on the d_{norm} surface, signifying close contacts, which originate from O-H...O or O-H...N interactions, comprising 5.0% and 20.4% of the total surface area for **1**_{MeCN} and **2**_{MeOH}, respectively. It is of interest to note that the contributions to the d_{norm} surface due to H...H contacts are 5.7% in **1**_{MeCN} and 18.5% in **2**_{MeOH}, implying vdW interactions being dominant for the supramolecular organization in **2**_{MeOH}. In addition, the small contributions of the other weak intermolecular C...C (3.2% for **1**_{MeCN} and 1.6% for **2**_{MeOH}), C...H/H...C (3.9% for **1**_{MeCN} and 0.4% for **2**_{MeOH}), C...O/O...C (3.8% **2**_{MeOH}), and H...N/N...H (8.3% for **1**_{MeCN}) contacts have negligible effects on the packing (Figure 7).

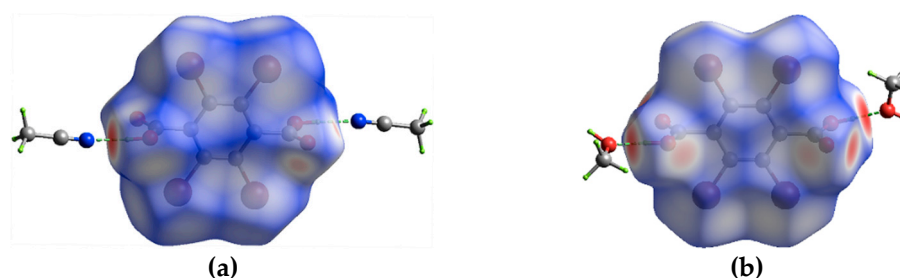


Figure 6. Illustration of the Hirshfeld surfaces mapped with d_{norm} for the intermolecular hydrogen bonding interactions between H₂Br₄tp and solvent molecules for (a) **1**_{MeCN} and (b) **2**_{MeOH}.

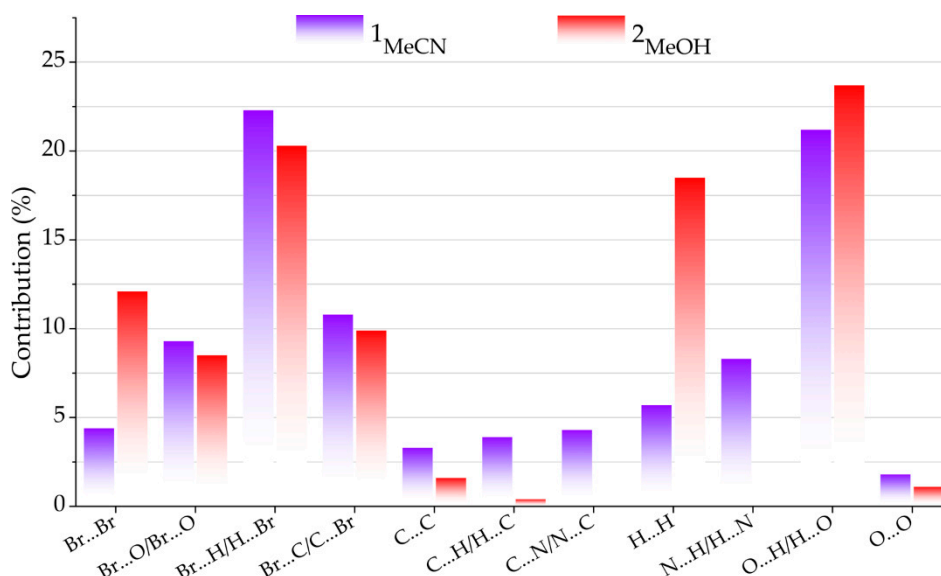


Figure 7. Quantitative results of different intermolecular contacts contributing to the Hirshfeld surfaces of the solvates.

3.3. Thermal Analysis and Structural Transformation

To evaluate the thermal behaviors of the solvates of $\text{H}_2\text{Br}_4\text{tp}$, TGA was performed on crystalline samples in the temperature range of 30 to 500 °C under nitrogen atmosphere. The TGA profiles of 1_{MeCN} , 2_{MeOH} , and $\text{H}_2\text{Br}_4\text{tp}$ are compared in Figure 8a. It was found that no weight loss was observed before 280 °C in the TGA curve of $\text{H}_2\text{Br}_4\text{tp}$, suggesting the absence of solvent molecules in its crystal structure. Meanwhile, the TGA curves of 1_{MeCN} and 2_{MeOH} show that the solvent (MeCN or MeOH) molecules are gradually lost from room temperature to $\approx 80\text{--}95$ °C, and then decomposition is observed beyond ≈ 250 °C.

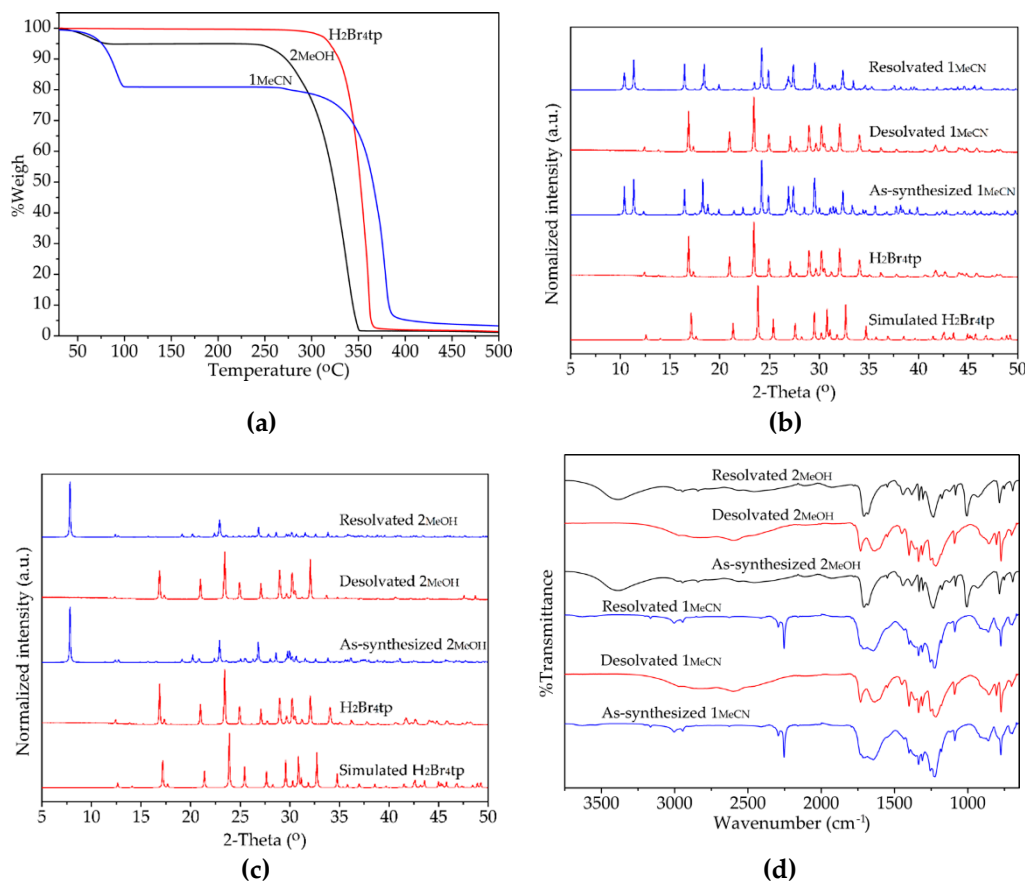


Figure 8. (a) Thermogravimetric analysis (TGA) curves of $\text{H}_2\text{Br}_4\text{tp}$, 1_{MeCN} , and 2_{MeOH} ; powder X-ray diffraction (PXRD) patterns (bottom to top) of simulated $\text{H}_2\text{Br}_4\text{tp}$, $\text{H}_2\text{Br}_4\text{tp}$, as-synthesized, desolvated, and resolvated crystals of (b) 1_{MeCN} and (c) 2_{MeOH} ; and (d) IR spectra (bottom to top) of as-synthesized, desolvated, and resolvated crystals of the solvates.

According to the TGA profiles, it is interesting that the structures of the host molecules remained intact after desolvation. Notably, PXRD patterns of the desolvated samples in Figure 8b,c also clearly reveal the formation of a new phase-pure material, in which the peak positions correspond well with $\text{H}_2\text{Br}_4\text{tp}$ in the monoclinic $C2/m$ space group [17]. Furthermore, the recyclability of the solvent release and resorption experiments was also examined. The crystalline samples of each solvate (≈ 10 mg) were placed in a crucible and heated at 110 °C under vacuum (≈ 10 mbar pressure) for 1 h. Indeed, the solvate form changes to the unsolvated phase, which can be confirmed by the disappearance of PXRD peaks at $2\theta = 10.40$ and 11.35° for 1_{MeCN} and at $2\theta = 7.83^\circ$ for 2_{MeOH} . Additionally, the absence of the solvent molecules was also evidenced by the disappearance of the $\text{C}\equiv\text{N}$ stretching vibration band of a nitrile group of MeCN ($\nu_{\text{C}\equiv\text{N}} = 2218 \text{ cm}^{-1}$) in the IR spectrum of 1_{MeCN} (Figure 8d) while only negligible changes could be observed in the IR spectrum of 2_{MeOH} . Both of the desolvated samples could be recovered to their original phase upon resorption with the corresponding solvent (MeCN or MeOH) and heating (110 °C, 1 h) in a Teflon-lined stainless autoclave. Alternatively, crystals of the original

phase can be obtained by simply immersing the desolvated samples in MeCN and MeOH solutions for 24 h. This reversible behavior can be repeated a number of times, which was confirmed by PXRD and IR spectroscopic techniques.

For a better understanding of the dynamic structural phase transition, detailed crystal structural information as well as intermolecular interactions of the desolvated crystals are very important. Although the desolvated crystals were found to possess similar morphologies to those of the original solvate forms and maintained their crystallinity, as confirmed by the PXRD experiments, they were found to diffract very poorly even at a medium resolution shell. Thus, single crystal structure determinations of these desolvated forms in this work were not possible. Despite several recrystallization attempts, regrettably, all failed to yield crystals of H₂Br₄tp alone. Fortunately, the solid-state structure of H₂Br₄tp determined from PXRD data was reported by Kumar et al. [17]. In packing, intermolecular O–H···Br hydrogen bonds are mainly responsible for the formation of a 2D sheet. Based on this evidence as well as our findings, we note that halogen bonding can be cooperative or competitive with hydrogen bonding during the desolvation–resolvation process.

4. Conclusions

In summary, H₂Br₄tp, a bromine and carboxyl-containing molecule, showed significant potential as a building block in the assembly of a 2D halogen-bonded sheet in crystalline state through a range of different halogen bonding synthons. These 2D assemblies can form 1:2 cocrystal solvates with MeCN and MeOH, in which the formation relies on very similar hydrogen bonding motifs between the respective components. Each solvate crystal showed distinct packing arrangements, which result from permutations of different halogen bonds. PXRD analysis and IR spectroscopy showed that the structural phase transitions between the solvated and the unsolvated crystals are reversible upon the release/resorption of solvent molecules. This study assessed the importance of the cooperative effect of halogen bonding in combination with hydrogen bonding interactions for engineering solvate crystals, permitting reversible release and resorption of solvent molecules.

Supplementary Materials: The following are available online at <https://www.mdpi.com/2073-4352/11/2/198/s1>. Table S1: Hydrogen bond geometry (Å, °) for **1**_{MeCN} and **2**_{MeOH}.

Author Contributions: Conceptualization, K.C.; funding acquisition, K.C. and M.S.; investigation, K.C. and M.S.; methodology, N.C., K.S., F.K., W.D., and K.C.; validation, K.C.; visualization, N.C., K.S., and K.C.; writing—original draft, K.C.; writing—review and editing, N.C., K.S., F.K., W.D., M.S., and K.C. All authors have read and agreed to the published version of the manuscript.

Funding: This project is mainly funded by the National Research Council of Thailand (NRCT5-RSA63010-01) and is also partially funded by the Thailand Research Fund (RTA6180007).

Institutional Review Board Statement: Not applicable.

Informed Consent Statement: Not applicable.

Data Availability Statement: Not applicable.

Acknowledgments: The authors also thank the Faculty of Science and Technology, Thammasat University, for funds to purchase the X-ray diffractometer. The Thammasat University Research Unit in Multifunctional Crystalline Materials and Applications (TU-MCMA) is also gratefully acknowledged.

Conflicts of Interest: The authors declare no conflict of interest.

References

1. Tiekink, E.R.T.; Vittal, J.J.; Zaworotko, M. (Eds.) *Organic Crystal Engineering: Frontiers in Crystal Engineering*; Wiley: Hoboken, NJ, USA, 2010.
2. Tiekink, E.R.T.; Zukerman-Schpector, J. (Eds.) *The Importance of π -Interactions in Crystal Engineering: Frontiers in Crystal Engineering*, 2nd ed.; Wiley: Hoboken, NJ, USA, 2012.
3. Desiraju, G.R. *Crystal Engineering: The Design of Organic Solids*; Elsevier: Amsterdam, The Netherlands, 1989.
4. Cavallo, G.; Metrangolo, P.; Milani, R.; Pilati, T.; Priimagi, A.; Resnati, G.; Terraneo, G. The halogen bond. *Chem. Rev.* **2016**, *116*, 2478–2601. [[CrossRef](#)]

5. Gilday, L.C.; Robinson, S.W.; Barendt, T.A.; Langton, M.J.; Mullaney, B.R.; Beer, P.D. Halogen bonding in supramolecular chemistry. *Chem. Rev.* **2015**, *115*, 7118–7195. [[CrossRef](#)]
6. Metrangolo, P.; Neukirch, H.; Pilati, T.; Resnati, G. Halogen bonding based recognition processes: A world parallel to hydrogen bonding. *Acc. Chem. Res.* **2005**, *38*, 386–395. [[CrossRef](#)] [[PubMed](#)]
7. Politzer, P.; Murray, J.S.; Clark, T. Halogen bonding: An electrostatically-driven highly directional noncovalent interaction. *Phys. Chem. Chem. Phys.* **2010**, *12*, 7748–7757. [[CrossRef](#)] [[PubMed](#)]
8. Cavallo, G.; Metrangolo, P.; Pilati, T.; Resnati, G.; Sansotera, M.; Terraneo, G. Halogen bonding: A general route in anion recognition and coordination. *Chem. Soc. Rev.* **2010**, *39*, 3772–3783. [[CrossRef](#)] [[PubMed](#)]
9. Priimagi, A.; Cavallo, G.; Metrangolo, P.; Resnati, G. The halogen bond in the design of functional supramolecular materials: Recent advances. *Acc. Chem. Res.* **2013**, *46*, 2686–2695. [[CrossRef](#)] [[PubMed](#)]
10. Mukherjee, A.; Tothadi, S.; Desiraju, G.R. Halogen bonds in crystal engineering: Like hydrogen bonds yet different. *Acc. Chem. Res.* **2014**, *47*, 2514–2524. [[CrossRef](#)] [[PubMed](#)]
11. Pop, L.; Grosu, I.G.; Miclăuș, M.; Hădăde, N.D.; Pop, A.; Bende, A.; Terec, A.; Barboiu, M.; Grosu, I. Halogen-bonded organic frameworks of perfluoroiodo- and perfluorodiodobenzene with 2,2',7,7'-tetrapyridyl-9,9'-spirobifluorene. *Cryst. Growth Des.* **2021**, *21*, 1045–1054. [[CrossRef](#)]
12. Dong, J.; Han, X.; Lui, Y.; Li, H.; Cui, Y. Metal-covalent organic frameworks (MCOFs): A bridge between metal-organic frameworks and covalent organic frameworks. *Angew. Chem. Int. Ed.* **2020**, *59*, 13722–13733. [[CrossRef](#)]
13. Liu, P.; Li, Z.; Shi, B.; Liu, J.; Zhu, H.; Huang, F. Formation of linear side-chain polypseudorotaxane with supramolecular polymer backbone through neutral halogen bonds and pillar[5]arene-based host-guest interactions. *Chem. Eur. J.* **2018**, *24*, 4264–4267. [[CrossRef](#)]
14. Liu, C.-Z.; Koppireddi, S.; Wang, H.; Zhang, D.-W.; Li, Z.-T. Halogen bonding directed supramolecular quadruple and double helices from hydrogen-bonded arylamide foldamers. *Angew. Chem. Int. Ed.* **2019**, *58*, 226–230. [[CrossRef](#)] [[PubMed](#)]
15. Schwabedissen, J.; Trapp, P.C.; Stammeler, H.-G.; Neumann, B.; Lamm, J.-H.; Vishnevskiy, Y.V.; Körte, L.A.; Mitzel, N.W. Halogen bonds of halotetrafluoropyridines in crystals and co-crystals with benzene and pyridine. *Chem. Eur. J.* **2019**, *25*, 7339–7350. [[CrossRef](#)] [[PubMed](#)]
16. Ji, B.; Zhang, D.; Liang, R.; Kang, G.; Zhu, Q.; Deng, D. Selective binding and removal of aromatic guests in a porous halogen-bonded organic framework. *Cryst. Growth Des.* **2021**, *21*, 482–489. [[CrossRef](#)]
17. Dey, S.K.; Saha, R.; Biswas, S.; Layek, A.; Middy, S.; Steele, I.M.; Fleck, M.; Ray, P.P.; Kumar, S. Tetrabromoterephthalic acid in designing co-crystals and salts: Modification of optical properties and Schottky barrier effect. *Cryst. Growth Des.* **2014**, *14*, 207–221. [[CrossRef](#)]
18. Bruker. *APEX3, SAINT and SADABS*; Bruker AXS Inc.: Madison, WI, USA, 2016.
19. Sheldrick, G.M. SHELXT—Integrated space-group and crystal-structure determination. *Acta Crystallogr. Sect. A Found. Adv.* **2015**, *71*, 3–8. [[CrossRef](#)]
20. Sheldrick, G.M. Crystal structure refinement with SHELXL. *Acta Cryst. Sect. C Struct. Chem.* **2015**, *71*, 3–8. [[CrossRef](#)]
21. Bondi, A. van der Waals Volumes and Radii. *J. Phys. Chem.* **1964**, *68*, 441–451. [[CrossRef](#)]
22. Etter, M.C.; MacDonald, J.C.; Bernstein, J. Graph-set analysis of hydrogen-bond patterns in organic crystals. *Acta Crystallogr. Sect. B Struct. Sci.* **1990**, *46*, 256–262. [[CrossRef](#)] [[PubMed](#)]
23. Chongboriboon, N.; Samakun, K.; Inprasit, T.; Kielar, F.; Dungkaew, W.; Wong, L.W.-Y.; Sung, H.H.-Y.; Ninković, D.B.; Zarić, S.D.; Chainok, K. Two-dimensional halogen-bonded organic frameworks based on the tetrabromobenzene-1,4-dicarboxylic acid building molecule. *CrystEngComm* **2020**, *22*, 24–34. [[CrossRef](#)]
24. Janiak, C. A critical account on π - π stacking in metal complexes with aromatic nitrogen-containing ligands. *J. Chem. Soc. Dalton Trans.* **2000**, 3885–3896. [[CrossRef](#)]
25. Spek, A.L. Platon Squeeze: A tool for the calculation of the disordered solvent contribution to the calculated structure factors. *Acta Crystallogr. Sect. C Struct. Chem.* **2015**, *71*, 9–18. [[CrossRef](#)] [[PubMed](#)]
26. McKinnon, J.J.; Jayatilaka, D.; Spackman, M.A. Towards quantitative analysis of intermolecular interactions with Hirshfeld surfaces. *Chem. Commun.* **2007**, 3814–3816. [[CrossRef](#)]
27. Spackman, M.A.; McKinnon, J.J. Fingerprinting intermolecular interactions in molecular crystals. *CrystEngComm* **2002**, *4*, 378–392. [[CrossRef](#)]
28. Turner, M.J.; Mckinnon, J.J.; Wolff, S.K.; Grimwood, D.J.; Spackman, P.R.; Jayatilaka, D.; Spackman, M.A. *CrystalExplorer17*; The University of Western Australia: Crawley, Australia, 2017.